DOI: 10.1002/ejic.201000967

Large-Scale, Surfactant-Free Solution Syntheses of $Cu(In,Ga)(S,Se)_2$ Nanocrystals for Thin Film Solar Cells

Jong Hyeon Lee,[a] Juyeon Chang,[b] Ji-Hyun Cha,[b] Yeji Lee,[b] Jae Eok Han,[b] Duk-Young Jung,*[b] Eun Chang Choi,[c] and Byungyou Hong[c]

Keywords: Sonochemical synthesis / Thin films / Nanoparticles / Electron microscopy / Solar cells / Photovoltaics

Large-scale (as much as 200 g in a batch) and surfactant-free syntheses of the $CuIn_xGa_{1-x}Se_2$ and the $CuIn_xGa_{1-x}S_2$ nanoparticles were investigated by employing a sonochemical process under ambient conditions. This synthetic approach eliminates the need for organic stabilizers, which may act as an insulator in the final device, and reduces the number of reaction steps for synthesis of high-quality CISe nanocrystals. We also demonstrate the solution-based fabrication of the thin film photovoltaic devices with a conversion efficiency of 2.62 % by using nanocrystal-based inks. The device was fabricated with 2 μm of a CIGS absorber layer on Mo-coated soda lime glass, 70 nm of a chemical-bath-deposited CdS layer, 100 nm of an intrinsic ZnO layer, followed by 800 nm of a Al-doped ZnO layer. Finally, a patterned Ag (200 nm) grid was deposited on the top of the device. The current results offer a promising alternative for solution-based CIGSe thin film solar cells, with a higher efficiency.

Introduction

Nanoscale chalcopyrite $CuIn_xGa_{1-x}Se_2$ (CIGSe) and $CuIn_xGa_{1-x}S_2$ (CIGS) have been identified as potentially promising materials for solution-based thin film solar cells because of the possibilities of large-area production and the significant cost-reduction in device fabrication.[1] Recently, several solution-based approaches with precursor solutions,[2] nanoparticle-based inks,[3] organometallic compounds,[4] and metal alloys[5] have been demonstrated for $Cu(In,Ga)(S,Se)_2$ thin film solar cell fabrication with high conversion efficiencies of up to 14%.[6] However, many issues have arisen with these approaches,[1,7] including the control of the composition of Ga for a higher efficiency device, the removal of the surfactants from the precursor materials for high-quality absorber layers, and, especially, the enlarging of the product quantity to significantly reduce fabrication costs. The tuning of the chemical composition of the CIGSe nanoparticles optimizes the conversion efficiency because the optical and electrical properties of the absorber layers strongly depend on the chemical stoichiometries of Cu-In-Ga-Se.[8] Since long hydrocarbon chains containing ligands are needed to synthesize monodispersed CISe nanoparticles,[9] the surfactant quantity governs the weight percentage of the prepared CISe nanoparticles, and thus eventually produces carbon residues resulting from the pyrolysis of the surfactants. Production of large quantities of high-purity CIGS nanoparticles with variable ternary or quaternary compositions is required prior to development of low-cost solution-based CIGS deposition techniques. Here, we present a facile route for the large-scale (≈200 g in a batch) and surfactant-free syntheses of $CuIn_xGa_{1-x}Se_2$ and the $CuIn_xGa_{1-x}S_2$ nanoparticles by employing a sonochemical process under ambient conditions. The sonochemical method has been used widely to generate nanosized materials because of the formation of particles with much smaller size and higher surface area.[10] In the current study, the ratio of indium and gallium and the size of the prepared particles could be controlled by varying the reaction conditions. This is the first report for the large-scale synthesis of high-purity ternary or quaternary $Cu(In,Ga)(S,Se)_2$ nanocrystals. We also demonstrate the solution-based fabrication of CIGSe thin film photovoltaic devices with a conversion efficiency of 2.62% through use of nanocrystal-based inks.

[a] Department of Chemistry, The Catholic University of Korea, Bucheon, Kyeonggi 420-743, Korea
[b] Department of Chemistry and Sungkyunkwan Advanced Institute of Nanotechnology, Institute of Basic Sciences, Sungkyunkwan University, Suwon 440-746, South Korea
Fax: +82-31-290-7075
E-mail: dyjung@skku.edu
[c] School of Information and Communication Engineering, Sungkyunkwan University, Suwon 440-746, Korea

Results and Discussion

A CISe nanocrystal was synthesized by employing a sonochemical process with Se powder, CuCl, and $In(OAc)_3$ in a mixture of hydrazine hydrate and ethylene glycol. The mixture with Se powder was black–brown because of the dissolution of Se in the hydrazine hydrate. When Cu and In sources were added to the mixture, the color of the solution became brown because of the formation of a Cu–Se and

In–Se phase. Finally, the solution turned deep black when CISe formed. The sonochemical process was performed under ambient conditions at 100 °C. This synthetic process does not need any surfactant because of the chemical effects achieved by ultrasound arising from acoustic cavitation.[10] CISe particles precipitated when the reaction was complete. A clear supernatant (i.e. no Se remained) was discarded, and its precipitate was washed with deionized water and ethanol by using a centrifugation. XRD data and Raman spectra of the four different $Cu(In,Ga)(S,Se)_2$ nanocrystals are shown in Figure 1. The XRD peaks for CISe at 26.6, 44.2, and 52.3 are indexed to (112), (220/204), and (321/116) reflections of the chalcopyrite structure, in which the observed peaks match well with the reference JCPD data (PDF #40–1487). The unit-cell parameters of CISe are $a = b = 5.788$ Å, $c = 11.641$ Å, shown in Table 1. The XRD peaks for the Ga-incorporated samples, CIGSe and CIGS, show a high angle shift and a large full width at half maximum (FWHM) values. The shift in the diffraction peaks is attributed to the decrease in the unit-cell parameters because of incorporation of Ga. The unit-cell parameters of CIGSe are $a = b = 5.682$ Å, $c = 11.344$ Å, shown in Table 1. In comparison to the CISe lattice parameters, the smaller values for the lattice constants obtained for the CIGSe nanocrystals may be caused by the partial substitution of In with Ga, which has a smaller atom size. The CIS and CIGS samples have smaller d values relative to those of the CISe and CIGSe samples, because of the smaller atom size of S than Se. The crystal sizes estimated with the Scherrer equation are 17 and 6 nm for CISe and CIGSe and 35 and 3 nm for the CIS and CIGS nanocrystals, respectively. The Raman spectra indicate a peak at about 170 cm^{-1} for CISe and CIGSe, which is a characteristic A_1 vibration mode from the $CuInSe_2$ phase. A shoulder at about 230 cm^{-1} is related to elemental Se, which is also revealed by the results of elemental compositions for the CISe and CIGSe samples in the Table 1. The peaks at about 290 cm^{-1} of CIS and CIGS predominantly correspond to the A_1 S–S vibrational mode from $CuInS_2$. The Raman spectra also show no Cu–Se or Cu–S phases.[11]

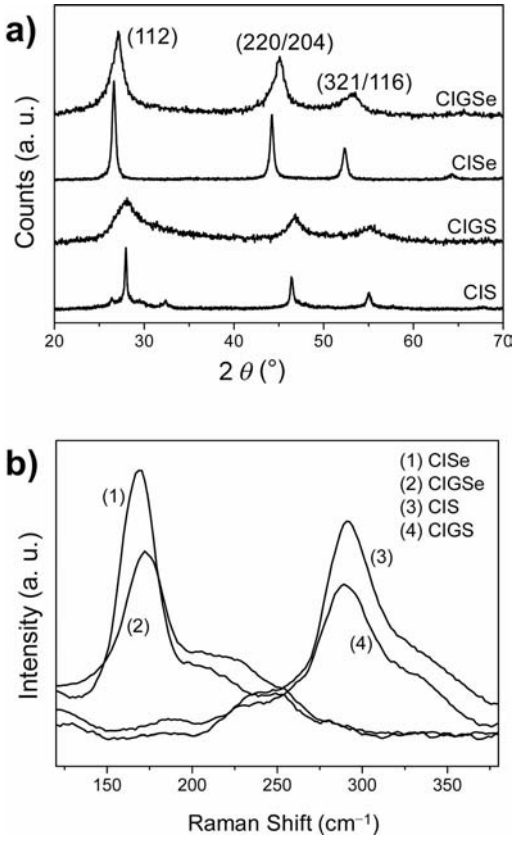

Figure 1. (a) XRD and (b) Raman spectra of $Cu(InGa)(S,Se)_2$ nanoparticles prepared by sonochemical synthesis. The samples are denoted as follows: $CuInS_2$ (CIS), $Cu(InGa)S_2$ (CIGS), $CuInSe_2$ (CISe), and $Cu(InGa)Se_2$ (CIGSe).

Table 1. Elemental compositions (atomic%) and lattice parameters of $Cu(In,Ga)(S,Se)_2$ nanoparticles.

Samples	Elemental composition [atomic%]				Lattice parameters [Å]	
	Cu	In	Ga	S or Se	*a*	*c*
CIS	22.8	26.3		50.8	5.550	10.871
CIGS	23.0	20.8	6.7	49.5	5.483	10.966
CISe	24.0	25.0		51.0	5.788	11.641
CIGSe	24.0	15.5	8.3	52.2	5.682	11.344

The SEM and HRTEM image of the CIGSe nanocrystals are shown in Figure 2. The high-resolution images of area 1 and 2 in Figure 2b can be seen in Figure 2c, d, respectively. The HRTEM images show lattice fringes that are well-matched to their XRD patterns, in which the d values of 0.20 nm and 0.32 nm in the Figure 2c, d correspond to the (220/204) and (112) peaks, respectively, of the CIGSe nanocrystals in Figure 1, respectively. The elemental maps for the CIGSe sample shown in Figure 3 also indicate a homogeneous distribution of Cu, In, Ga, and Se. It can clearly be seen that for all samples, high-purity ternary or quaternary $Cu(In,Ga)(S,Se)_2$ nanocrystals can be achieved by using this sonochemical process. Carbon impurities are

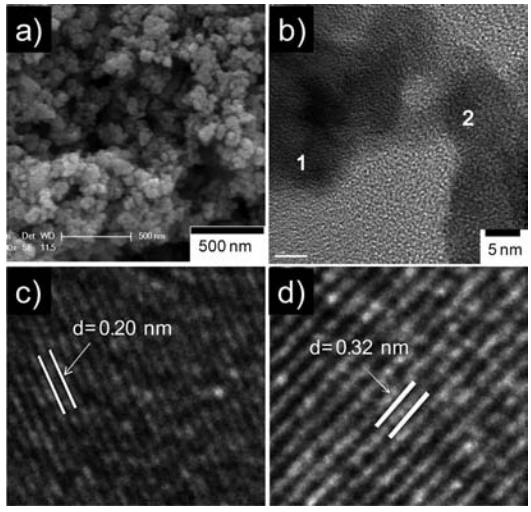

Figure 2. (a) SEM and (b–d) HRTEM images of the $Cu(InGa)Se_2$ nanocyrstals; (c) and (d) are high-resolution images of areas 1 and 2 in (b).

detected within the error of EDX (data not shown), because we did not employ the organic stabilizers, which may act as an insulator in the final device.

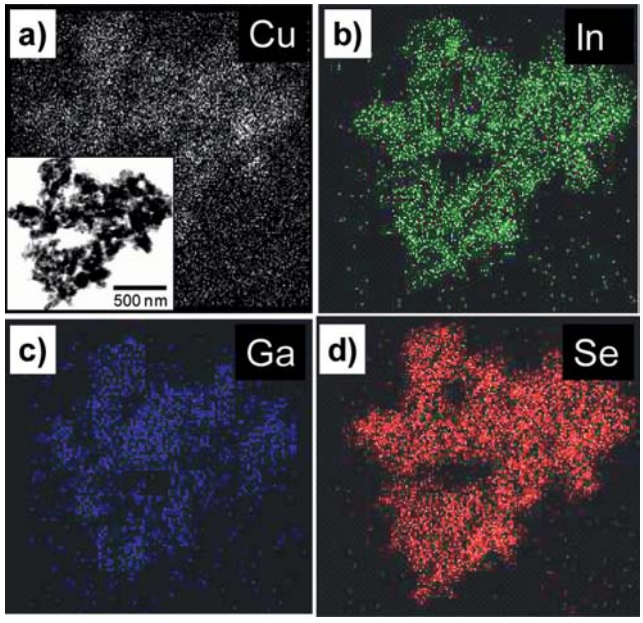

Figure 3. Elemental maps of the Cu(InGa)Se_2 nanocyrstals. Inset in (a) indicates the TEM image of the nanocrystals.

In order to prepare an ink solution, the as-prepared nanocrystal CIGSe was dispersed in hydrazine hydrate, where the typical concentration of the ink was ca. 150 mg/mL. Prior to depositing the CIGSe ink solution, the mixture was constantly stirred for 6 h and yielded a homogeneous colloidal solution. We employed spin coating as a representative solution-based process for the deposition of the precursor ink solution. The film deposition process was performed in an argon-filled glove box. The CIGSe ink was spin cast onto Mo-coated (500 nm thick and 2 cm × 2 cm area) soda lime glass, and the films were then immediately dried at 300 °C, which is a process similar to that in the previous report.[2a] The 1.94-μm thick CIGSe absorber layer was deposited by using several deposition cycles and a selenization process with a load-lock tube furnace at 475 °C for 25 min. Residual selenium was removed during post-annealing at 450 °C for 5 min by a rapid thermal process (RTP). The device was completed with a 70-nm thick layer of chemical-bath-deposited CdS[12] and ZnO, followed by 800 nm of an Al-doped ZnO layer (AZO).[13] The sheet resistance of the AZO layer (on a glass plate) was ca. 50 Ω/sq, which was measured by using the 4-point probe method. Finally, a patterned Ag (200 nm) grid was deposited on the top of the device. Each cell was isolated by mechanical scribing, the active area of the device was 0.262 cm^2. Current/voltage (*I*–*V*) measurements were carried out by using a Wacom WXS-155S-L2 (class-AAA) solar simulator under Korea Institute of Energy Research (KIER) calibrated AM 1.5 global with an intensity of 100 mW/cm^2 at 25.0 °C.

The SEM images of the predeposited and selenized CIGSe thin films are shown in Figure 4. After the selenization process, up to 500 nm of the predeposited nanoparticles were crystallized, with an average value of 200 nm, and the surface cracks were removed. The XRD data of selenized CIGSe films on Mo-coated soda lime glass were indexed to the reflections of the $CuInSe_2$ crystal structure. The crystalline sizes of the predeposited and the selenized films estimated with the Scherrer equation are 15 and 195 nm, respectively, and the estimated grain size shows good agreement with the average particle size from SEM. The average composition of the selenized film determined by EDX is $Cu_{0.82}In_{0.68}Ga_{0.25}Se_2$, where Cu/(In+Ga) is 0.88. The film was maintained at a Cu-poor composition with a Cu/(In + Ga) atomic ratio of less than one. It is clear that the annealing process under Se pressure was dominantly effective for the grain growth of the quaternary Cu(In,Ga)-Se_2 absorber layer.

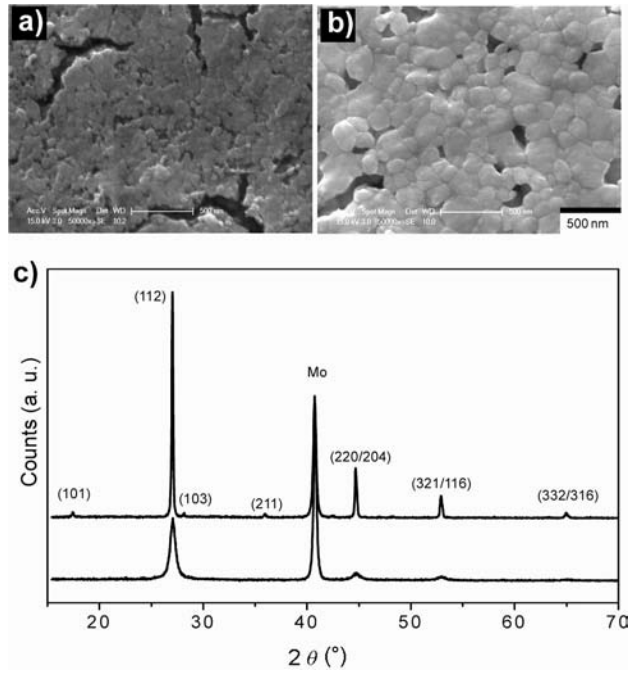

Figure 4. SEM images of (a) as-coated and (b) selenized Cu(InGa)-Se_2 thin films. (c) XRD peaks of as-deposited (lower pattern) and selenized Cu(InGa)Se_2 thin films (upper pattern) on Mo-coated soda lime glass.

A cross-section SEM image and top view of the final device with the CIGSe absorber layer is shown in Figure 5. The grain structures of a selenized Cu(InGa)Se_2 absorber layer with a thickness of 1.94 μm and ca. 100 nm of the Mo–Se interfacial layer can be seen in Figure 5a. The thin Mo–Se layer has been reported in vacuo-deposited CIGSe films and may be beneficial for an increase in Ohmic contact between the CIGSe and Mo layer.[14] Optical absorption measurements were performed on the 100-nm thick CIGSe absorber layer on a 1-mm thick soda lime glass (data not shown). The sample was annealed by using a load-lock tube furnace under Se atmosphere at 475 °C for 25 min. The estimated band gap of the CIGSe layer is approximately 1.10 eV. The quantum efficiency (%) and *I*–*V* characteristics of a typical solar cell fabricated with the se-

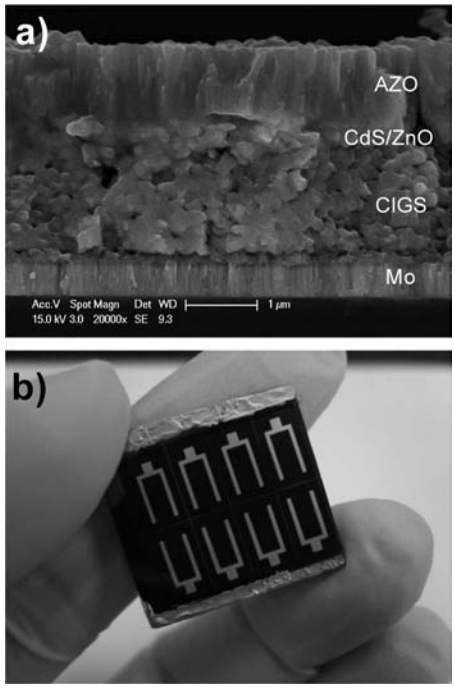

Figure 5. (a) Cross-sectional SEM image and (b) top view of a $CIGSe_2$-based solar cell device.

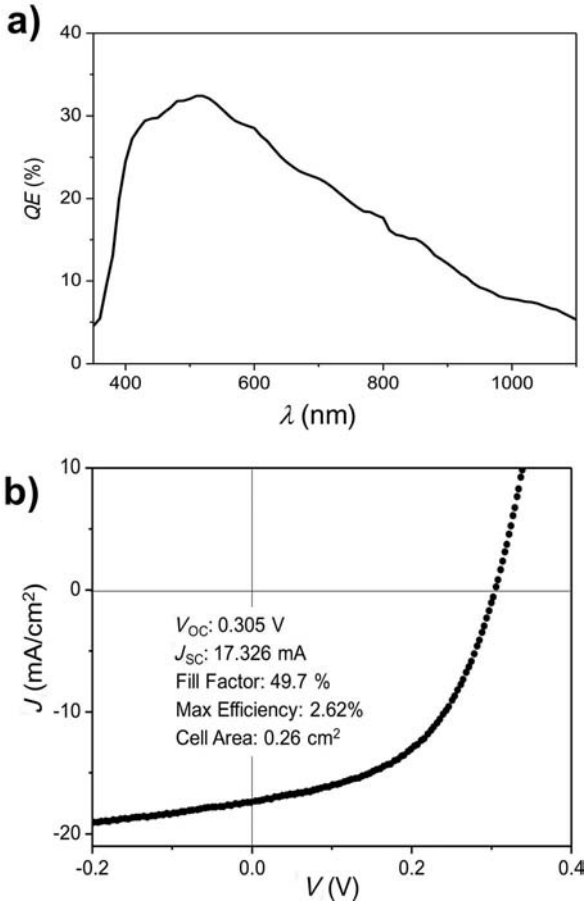

Figure 6. (a) QE and (b) *I–V* characteristics of the final Cu(InGa)Se_2 device. The device was scribed into small area devices (≈0.26 cm^2), and the efficiency of the cell was calculated per active area by excluding the shaded area.

lenized Cu(InGa)Se_2 absorber layer is shown in Figure 6. The low quantum efficiency may be ascribed to the smaller grain structures of the Cu(InGa)Se_2 absorber layer than those of other CIGSe-based devices. The device exhibits an efficiency of 2.62% for illumination with a solar simulator having an intensity of 100 mW/cm^2. The device characteristics are V_{OC} = 0.305 V, J_{SC} = 17.326 mA, and FF = 49.7% on 0.262 cm^2 of active area. The V_{OC} in the current device was lower than that of the high-efficiency solar cells.[2] The FF was higher than that of other CIGSe-based devices prepared by using a mechanochemical/screen printing method.[3c] Therefore, overall cell performance of the current device is comparable to other non-vacuum-based techniques.

Conclusions

A novel, facile, and large-scale synthesis of $CuInGaSe_2$ and the related chalcopyrite nanoparticles was investigated by use of the sonochemical method with a hydrazine-based solvent that strongly induces the incorporation of Ga into the crystalline lattice of CIS and CISe. This synthetic approach eliminates the need for organic stabilizers, which may act as an insulator in the final device, and reduces the number of reaction steps for the synthesis of high-quality CISe nanocrystals. With regard to the nanocrystal ink, a simple process for device fabrication by using a non-vacuum technique based on the selenized Cu(In,Ga)Se_2 absorber layer is presented. The photovoltaic device of the quaternary CIGSe nanoparicles exhibits a solar conversion efficiency of 2.62%. By varying the deposition techniques, the current results offer a promising alternative for solution-based CIGSe thin film solar cells, while yielding a higher efficiency.

Experimental Section

Synthesis of $CuInGaSe_2$ Nanoparticles: CuCl (0.6 mol), $In(OAc)_3$ (0.42 mol), $Ga(NO_3)_3{\cdot}xH_2O$ (0.18 mol), and Se powder (1.2 mol) were mixed with ethylene glycol and hydrazine monohydrate (98%). (**Warning:** We note that hydrazine monohydrate is toxic and may be fatal if inhaled, swallowed, or absorbed through the skin, and therefore should be handled with personal protective equipments to prevent contact.) For Cu(In,Ga)S_2, a sulfur powder was employed instead of Se. The mixture was stirred under a high-power ultrasonic generator (Hielscher Ultrasonic GmbH) for 3 h under ambient conditions at 110 °C. The product was centrifuged and washed with degassed water several times and dried at room temperature for further characterization. Coating of the CIGSe absorber layers involves the dispersion of the prepared nanoparticles in hydrazine hydrate, spin-casting of the precursor ink, and finally heating of the CIGSe film with selenium powder under argon for 30 min at below 500 °C.

Characterization: X-ray diffraction (XRD) patterns of both powder samples and thin films deposited on Mo-coated glass were measured with a Rigaku X-ray diffractometer, D/MAX-2000 Ultima, in the θ–2θ scanning mode at 40 kV and 30 mA by using Cu-K_α radiation (λ = 1.5405 Å). The scanning electron microscopy (SEM) images were obtained on a JEOL 7401F instrument (JEOL Ltd, Japan) operating at 30 kV. Before imaging, the samples were

coated on carbon by sputtering with Pt, to a thickness of about 3 nm. The high-resolution transmission electron microscopy (HRTEM) images were taken on a JEOL 300 KV instrument (JEOL Ltd. Japan). Raman spectra were measured at 514 nm with a Renishaw micro-Raman spectrometer. The UV/Vis absorption measurements were carried out with a S3100 (Sinco) instrument. The current/voltage (*I–V*) measurements were carried out by using a Wacom WXS-155S-L2 (class-AAA) solar simulator under Korea Institute of Energy Research (KIER) calibrated AM 1.5 global with an intensity of 100 mW/cm^2 at 25.0 °C.

Acknowledgments

This work was funded by the Technology Development Program for New and Renewable Energies (KETEP-2009-3021010030), the National Research Laboratory Program (NRF-2010-0018917), the Priority Research Center Program (NRF-2009-0094025) and the Basic Science Research Program through HINT (NRF-2010-0015035).

[1] a) D. L. Schulz, C. J. Curtis, R. A. Flitton, H. Wiesner, J. Keane, R. J. Matson, K. M. Jones, P. A. Parilla, R. Noufi, D. S. Ginley, *J. Electron. Mater.* **1998**, *27*, 433–437; b) M. Kaelin, D. Rudmann, A. N. Tiwari, *Sol. Energy* **2004**, *77*, 749–756.

[2] a) D. B. Mitzi, M. Yuan, W. Liu, A. J. Kellock, S. J. Chey, V. Deline, A. G. Schrott, *Adv. Mater.* **2008**, *20*, 3657–3662; b) W. W. Hou, B. Bob, S. Li, Y. Yang, *Thin Solid Films* **2009**, *517*, 6853–6856.

[3] a) V. K. Kapur, A. Bansal, P. Le, O. I. Asensio, *Thin Solid Films* **2003**, *431–432*, 53–57; b) M. Kaelin, D. Rudmann, F. Kurdesau, H. Zogg, T. Meyer, A. N. Tiwari, *Thin Solid Films* **2005**, *480–481*, 486–490; c) T. Wada, Y. Matsu, S. Nomura, Y. Nakamura, A. Miyamura, Y. Chiba, A. Yamada, M. Konagai, *Phys. Status Solidi A* **2006**, *203*, 2593–2597; d) Q. Guo, G. M. Ford, H. W. Hillhouse, R. Agrawal, *Nano Lett.* **2009**, *9*, 3060; e) L. Li, N. Coates, D. Moses, *J. Am. Chem. Soc.* **2010**, *132*, 22–23.

[4] J. A. Hollingsworth, K. K. Banger, M. H.-C. Jin, J. D. Harris, J. E. Cowen, E. W. Bohannan, J. A. Switzer, W. E. Buhro, A. F. Hepp, *Thin Solid Films* **2003**, *431–432*, 63–67.

[5] G. Norsworthy, C. R. Leidholm, A. Halani, V. K. Kapur, R. Roe, B. M. Basol, R. Matson, *Sol. Energy Mater. Sol. Cells* **2000**, *60*, 127–134.

[6] Nanosolar Inc., PVSEC 17, Tokyo, Japan, **2007**. (available at http://www.nanosolar.com/cache/PVSEC17_ns_dft.pdf).

[7] T. Todorov, D. B. Mitzi, *Eur. J. Inorg. Chem.* **2010**, 17–28.

[8] a) T. Markvart, L. Castaner, *Solar Cells (Materials, Manufacture and Operation)*, Elsevier, UK, **2005**, pp. 303–349; b) R. H Bube, *Photovoltaic Materials (Series on Properties of Semiconductor Materials*, Vol. 1), Imperial College Press, UK, **1998**, pp. 184–224; c) S. Ahn, K. Kim, J. Yun, J. Lee, K. Yoon, *Sol. Energy Mater. Sol. Cells* **2007**, *91*, 1836–1841.

[9] M. A. Malik, P. O'Brien, N. Revaprasadu, *Adv. Mater.* **1999**, *11*, 1441–1444.

[10] a) J. Zhu, Y. Koltypin, A. Gedanken, *Chem. Mater.* **2000**, *12*, 73–78; b) J. Y. Park, J. P. Park, C. H. Hwang, J. Kim, M. H. Ho, K. M. Ok, H. Y. Kwak, I. W. Shim, *Bull. Korean Chem. Soc.* **2009**, *30*, 2713–2716.

[11] V. Izquierdo-Roca, E. Saucedo, C. M. Ruiz, X. Fontané, L. Calvo-Barrio, J. Álvarez-Garcia, P.-P. Grand, J. S. Jaime-Ferrer, A. Pérez-Rodríguez, J. R. Morante, V. Bermudez, *Phys. Status Solidi A* **2009**, *206*, 1001–1004.

[12] M. A. Contreras, M. J. Romero, B. To, F. Hasoon, R. Noufi, S. Ward, K. Ramanathan, *Thin Solid Films* **2002**, *403–404*, 204–211.

[13] S. Ishizuka, K. Sakurai, A. Yamada, K. Matsubara, P. Fons, K. Iwata, S. Nakamura, Y. Kimura, T. Baba, H. Nakanishi, T. Kojima, S. Niki, *Sol. Energy Mater. Sol. Cells* **2005**, *87*, 541–548.

[14] T. Wada, N. Kohara, S. Nishiwaki, T. Negami, *Thin Solid Films* **2001**, *387*, 118–122.

Received: September 10, 2010
Published Online: January 5, 2011

